JOURNAL OF OPTOELECTRONICS AND ADVANCED MATERIALS, Vol. 11, No. 2, February 2009, p. 104 - 113

Linear and nonlinear optical properties of the CdSe nanocrystals embedded in PMMA matrix

A. CHAIEB[a,b], O. HALIMI[b], A. BENSOUICI[b], B. BOUDINE[b], B. SAHRAOUI[a*]
[a]*Laboratory POMA, FRE CNRS 2988, University of Angers, 2, Boulevard Lavoisier, 49045 Angers, France*
[b]*Laboratory of Crystallography, Department of Physics, University of Constantine, road Ain El bey 25000, Algeria*

CdSe nanocrystals (NCs) were prepared using a colloidal solution and dispersed in polymethylmethacrylate (PMMA) matrix. Using spin coating technique, thin films deposited on glass substrates were prepared. Their structural and optical properties were investigated by X-ray diffraction, atomic force microscopy (AFM) and UV-visible absorption, respectively. The absorption spectra of these dispersed NCs exhibit excitonic peaks resulting from the electron-hole coupling transitions. Due to a quantum confinement effect, a blue shift is deduced by comparison of such transition with respect to reported bulk band gap. Assuming a spherical like shape for these NCs, the crystallites radius (R) was estimated by applying the effective mass approximation model and was about 2.92 nm. Such a weak radius value compared to Bohr radius (R_B = 5.5 nm) leads to a strong quantum confinement regime. Moreover, the influence of this confinement effect on nonlinear optical (NLO) properties was also studied. Quadratic and cubic NLO properties were investigated by second and third harmonic generation techniques (SHG and THG) with a Q-switched Nd:YAG laser working at 1064 nm fundamental wavelength. The NLO susceptibilities $\chi_{eff}^{<2>}$, $\chi_{eff}^{<3>}$ were measured to be equal to $2.27.10^{-10}$(m/V) and $2.28.10^{-20}$(m^2/V^2), respectively.

(Received February 5, 2009; after revision February 20, 2009; accepted February 24, 2009)

Keywords: Nonlinear Optics, Nanocrystals, CdSe, PMMA, THG, SHG, Exciton, Quantum confinement.

1. Introduction

II–VI semiconductors nanocrystals (NCs) have been intensively studied in recent years due to their interesting properties and potential applications. Lowering the system dimensions to nanometric scale give rise to very promising and unique properties that can be applied in optoelectronics and photonics devices such as laser diodes [1-2], frequency doublers, solar cells, electron–beam pumped lasers, optical devices [3] and also used as biological tags [4-5]. The NCs doped thin films can be prepared by various deposition techniques like chemical vapour deposition (CVD), sputtering, electro deposition, vacuum evaporation, sol-gel process and colloidal solution. These semiconducting nanoparticles have attracted considerable interest due to their size dependent physical properties [6-8]. Particularly, CdSe NCs are considered as a reference material for investigation of fundamental physical properties of II-VI semiconductors NCs. They are reported to be a state of matter in the transition region between atom and bulk solid.

CdSe bulk exhibits band gap energy of 1.74 eV that corresponds to an absorption edge of 690 nm. Because of the quantum confinement that affects strongly the optical properties of the films, the CdSe NCs can display a size dependence of the absorption edge [9].

In this paper we report linear and nonlinear optical properties (optical absorption, generation of the second and third harmonic) of CdSe NCs dispersed in a PMMA matrix by colloidal solution and deposited on a glass substrate using spin coating technique. The low dimension of NCs size induces a quantum confinement effect leading to the size dependence of the band gap energy described well by the effective mass approximation (E.M.A) [10-11].

2. Experimental

2.1. Preparation

CdSe nanoparticles doped polymer system was prepared by colloidal solution. A host solution was prepared by dissolving amorphous polymer PMMA in tetrahydrofuran (THF) with a concentration of 0.02 g/ml. This solution was stirred at 50°C for 2 hours. A guest solution was prepared with 0.153 g of mechanically crushed CdSe powder dispersed in 5 ml of THF. Finally, both solutions were blended together and stirred.

Glass slabs used as a substrate were degreased, rinsed thoroughly with distilled water before deposition of few droplets of NCs CdSe doped PMMA solution. Thin films were deposited by spin coating technique performed under various conditions depending on the viscosity of the mixture. The rotational speed ranged from 300 to 2000 rpm in order to control the thickness. The deposition principle is based on homogeneous spreading using appropriate conditions.

All experiments were performed at room temperature and ambient pressure. The thicknesses of the films were mechanically measured using a Dektak stylus profiler 6 M (Veeco).

2.2. X ray diffraction

X-ray diffraction patterns of the CdSe NCs doped PMMA films were measured using an X-ray diffractometer model D8 Advance, Bruker with Ni filtered Cu radiation generated at 30 kV and 30 mA (CuKα =1.542 Å) as the X-ray source. Film samples were cut into rectangular pieces (1cm×2 cm), mounted on the holder and used for analyses. The diffraction patterns were determined over a range of diffraction angles 2θ = 10 to 85° at a rate of 2° (in 2θ) per minute.

2.3. UV spectrum

The absorption spectrum of the thin films was recorded using a UV-visible/NIR spectrophotometer (Perking Elmer, model Lambda 19) in the spectrum range from 200 to 1000 nm.

2.4. AFM measurements.

The AFM images were recorded in tapping mode at a scan rate of 1Hz with a CP Research (Thermomicroscope/Veeco, Dourdan, France). The image processing was performed using the WSxM 4.0 program (Nanotec, Spain). Analysis by AFM offers the ability to establish elementary characteristic values such as the thickness of film and the surface homogeneity.

2.5. Nonlinear optical properties

2.5.1. SHG measurements

Second order NLO susceptibility of the studied compounds was investigated by second

Harmonic generation experiments in transmission. The experimental setup of the SHG technique is presented in figure 1. As a source the Nd: YAG laser (model Continuum Leopard D-10) was used. It provides 16 ps pulses of several mJ, at 1064 nm wavelength, with a frequency of 10 Hz. Two separating beam splitters (BS) are sampling one part of incidental beam on a first photodiode (Motorola MRD500; Ph_s) for synchronizing the acquisition, and on second photodiode (Hamamatsu S1226-8BK; Ph_c) for sampling the energy of fundamental beam. A system half-wave (λ/2) plate and Glan polarizer (P) allows, to vary the energy of the incident beam. A convergent lens (L), with the focal distance of 250 mm, allows focusing the beam on a sample with its rotation axis placed near the focus of this lens. Samples were placed on a rotational stage (model Standa 8MR180) which allows rotating sample with high precision. A selective filter KG3 (F) cuts the fundamental wavelength transmitted at 1064 nm and allow passing the harmonic generated. A second interferential filter FL532 permits to preserve only the second harmonic at 532 nm (±1 nm). This filter is placed inside of the photomultiplier (Hamamatsu R1828-01; PMT), which measures second harmonic signal intensity. For each sample, the measurements of the second harmonic signal intensity as a function of the incidental angle is performed on a total of 50 laser impulses for each angular position. The change of the incident angle is generally made from -50° to +50° round the normal of incidental beam per step of 0.2°. The angular dependence of the SHG intensity leads to the so-called Maker fringes [12-13]. The experiment was calibrated using a y-cut crystalline quartz plate used as standard reference for quadratic NLO effects in thin films.

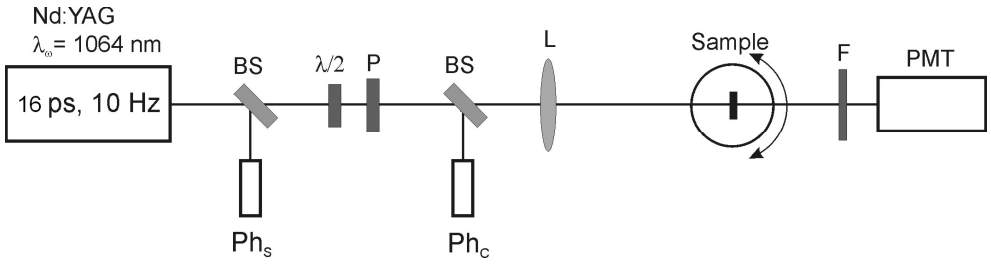

Fig. 1. SHG and THG experimental setup: BS beam splitters; Phs: synchronization photodiode; λ/2: half wave plate; P: Gland polarizer; Phc: control photodiode; L: convergent lens; F: selective filter (532 nm for SHG and 355 nm for THG); PMT:photomultiplier tube.

2.5.2. THG measurements

Third order NLO susceptibility of the studied compounds was evaluated by third harmonic generation (THG) experiments in transmission mode [14-15], (see figure 1). We used the same experimental arrangement as previously described in SHG experiment. The only difference for the THG measurements was the change of the interferential filter to 355 nm before reaching the photomultiplier tube. The experiment was calibrated using a 1 mm thick silica plate used as reference for cubic NLO effects in thin films.

3. Results and discussion

3.1. X-ray diffraction analysis

The X-ray diffraction (XRD) patterns of CdSe-PMMA guest host films (see figure 2) point the nanometric scale of the incorporated CdSe particles and its

wurtzite (hexagonal) structure belonging to the 6_{mm} space group. The crystallites are preferentially oriented with the (002) planes parallel to the substrate surface. Table 1 lists the characteristic lines versus 2θ of the compound. The XRD patterns exhibit sharp peaks at 2θ equal to: 23.589°, 24.990°, 26.746°, 41.620° which correspond respectively to the (100), (002), (101), (110) hexagonal phase (wurtzite) diffraction planes. By comparing this result, with the XRD patterns of CdSe powder assigned by a standard JCPDS database file n° 08-0459. One can notice a shift of peaks and also a considerable broadening, indicating low dimensions of the incorporated nanocrystallites CdSe in the PMMA matrix.

This broading of the peaks is an evidence of the small size of the CdSe particles. The average radius of the dispersed particles in the PMMA matrix was estimated using the Scherrer formula (E 1) in which the crystallites are assumed to possess a spherical shape.

$$2R = \frac{0.89\lambda}{\Delta\theta\cos(\theta)} \quad (1)$$

R is particle radius, λ corresponds to CuKα tube wavelength emission, θ is the diffracted angle and $\Delta\theta$ the full width at half maximum (FWHW) in radians of the peak. The calculated average value of the size of the particles was about 8.56 nm (Table 2) justifying hence the nanometric size of the particles.

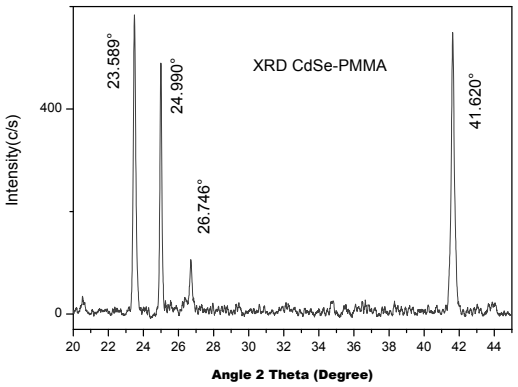

Fig. 2. X-ray diffraction patterns of CdSe-PMMA nanocomposite thin film.

Table 1. XRD data of CdSe NCs doped PMMA and pure CdSe powder.

2θ (°) (CdSe-PMMA)	Intensity (%) CdSe-PMMA	2θ (°) (CdSe powder) (wurtzite)	Intensity (%) CdSe powder	Diffraction planes
23.589	100	24.04	75	(100)
24.990	82.7	25.54	85	(002)
26.746	18.9	27.31	35	(101)
41.620	85.4	42.02	100	(110)

Table 2. CdSe NCs Radius calculation using the Scherrer formula (E 1).

2θ (°)	Diffraction planes	Δθ (°) Full width at half maximum (FWHM)	Radius size (nm) (R)
23.589	(100)	0.490	9.353
24.990	(002)	0.462	9.451
26.746	(101)	0.641	6.981
41.620	(110)	0.620	8.481

3. 2. Optical analysis of the CdSe NCs-PMMA system

3. 2.1. Absorption

The absorption spectrum represents a signature of the studied material. Polymethylmethacrylate polymer was used as host matrix because of its transparency in the visible wavelength range. Figure 3 shows the optical absorption spectrum of the CdSe NCs-PMMA system versus the wavelength. The observed spectrum exhibits absorption band edges at 535 nm, and excitonic absorption peaks at 500 nm and .470 nm. That dependent upon the size of the CdSe NCs .Furthermore the absorption edge shifts to the shorter wavelengths. Such trend is in good agreement with the work of T. Arai et al [16]. From the data of Murray et al [9], the edge around 550 nm in the absorption spectrum corresponds to CdSe nanoparticles with a diameter of 3.7 nm. The optical band gap energy that is related to the position of the lowest absorption maxima was evaluated from the minimum of the second derivative of the absorption spectrum [17-18]. Optical band gap energy increases with a corresponding decrease of crystallite size. By this method, E^*=2.31eV was obtained for the first allowed transition energy that corresponds to the optical band gap energy, attributed to the ground state ($1S_{3/2}$, $1S_e$), i.e. the lowest electron–hole energy between the quantized interior states of NCs (HUMO-LUMO), which we refer to as band-edge exciton.

Taking into account the first transition energy of the film E^* (CdSe-PMMA) = 2.31 eV and the band gap energy of the bulk CdSe Eg = 1.74 eV [19], the quantum confinement energy ΔE was estimated by the relation ΔE = E^* - Eg and is equal to 0.57 eV. From this variation of energy, the particle size can be calculated. The size effects can be deduced from Schrödinger's equation in quantum mechanical theory for which the exciton can be described by the Hamiltonian,

$$H = \frac{\hbar^2}{2m_h^*}\Delta_h - \frac{\hbar^2}{2m_e^*}\Delta_e - \frac{e^2}{\varepsilon|r_e - r_h|} \quad (2)$$

The wave function and the energy states of the exciton can be determined. From the wave function, the energy of

the lowest excited state is given by the model of the effective mass approximation with a contribution of coulomb interaction developed by Kayanuma [20] and Brus [21]

$$E^*(R) = E_g + \frac{\hbar^2\pi^2}{2R^2}\left(\frac{1}{m_e^*} + \frac{1}{m_h^*}\right) - \frac{1.786e^2}{\varepsilon R} - 0.248E_{Rey} \quad (3)$$

where $E^*(R)$ the optical band gap energy and E_g is the bulk band gap energy. The second term involving the electron and hole effective masses m_e^* and m_h^* respectively, corresponds to the exciton kinetic-energy. ε is the dielectric constant of the material. The third term involving ε arises due to the Coulomb attraction between the electron and the hole, and the last term is due to the spatial correlation between the electron and the hole and is generally small compared to the others terms.

For CdSe: $m_e^* = 0.13\ m_0$, $m_h^* = 0.45\ m_0$ [22], $\varepsilon = 10$ and m_0 is the free electron mass. The average radius of NCs inside the thin film is estimated to be 2.92 nm.

Such result shows that the decreasing of the crystallites size leads to an enhancement of the optical gap energy. By comparing the CdSe NCs average size to the Bohr radius of the exciton which is about $r_B = 5.5$ nm, we obtain $R < r_B$ corresponding to a strong confinement regime. This result is in good agreement with those reported by Murray et al [9] and Miroslav Šimurda et al [23].

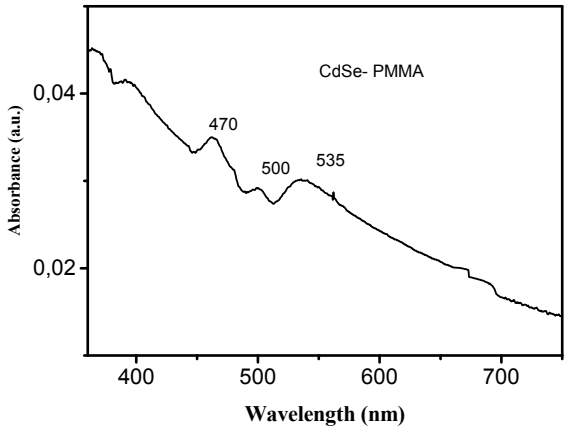

Fig. 3. Absorption spectra of CdSe-PMMA nanocrystals. The average size of CdSe nanocrystals was estimated to be 2.92 nm. Exciton absorption peaks at 470, 500 nm and the absorption band edge at 535nm.

3. 2.2. Principle of the second harmonic generation

The second harmonic generation (SHG) consists in generating a wave of twice frequency 2ω starting from an incident beam of frequency ω. In fact, the second harmonic generation represents an optical interaction in which two photons of energy $h\nu$ (in our case $\lambda_\omega = 1064$ nm and ($h\nu$ = 1.17eV) interacting with the nonlinear material are combined to form a new photon of energy $2h\nu$ (here $\lambda_{2\omega} = 532$ nm and $2h\nu$ = 2.34 eV). This method has been especially developed in order to determine the value of second order nonlinear susceptibility of a non-centrosymmetric material by measuring the change in second harmonic intensity versus the incidence angle (see figure 8). Actually, when the incidence angle is varied, the length of the optical pathway within nonlinear material is varied as well. When the thickness of the material d is higher than the coherence length L_c, the wave's *constraint* and *free* interfere to each other and the intensity of second harmonic signal can pass through a series of maxima and minima called the *Maker fringes* [24].

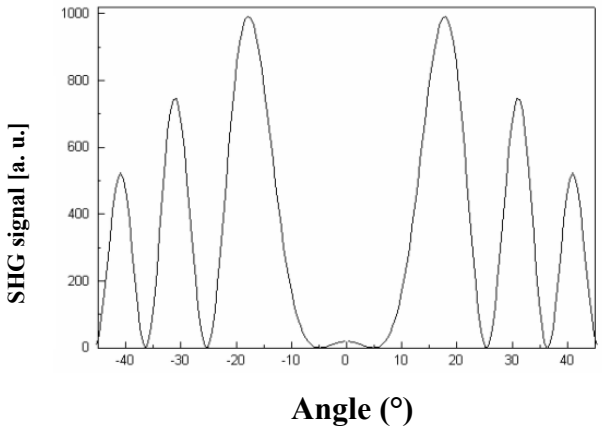

Fig. 4. An example of second harmonic signal as function of the incidence angle θ_i.

Maker fringes become closer with the increase of incidence angle $|\theta_i|$ since the interaction length is rising in a nonlinear manner with $|\theta_i|$ while the fringe intensity is going down, since the losses caused by reflexion are increasing with the increase of $|\theta_i|$.

The Maker's fringes characterise the change in the length of the interaction length when this is subjected to a rotational movement (see figure5). The interaction length (L) is given by the following relation:

$$L = \frac{d}{\cos\theta_t} \text{ with } \theta_t = arcsin\left[\frac{\sin\theta_i}{n_0}\right], \quad (4)$$

Where d denotes the thickness of the material and n_0 is the refractive index of the medium.

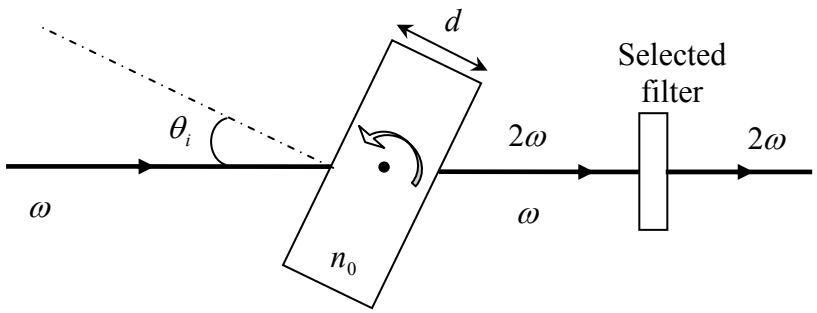

Fig. 5. The principle of SHG technique.

The change in interaction length determines a change in the phase mismatch $\Delta\Psi$ between the waves constrained and free. In isotropic media the refractive index show a normal dispersion, and then $n_{2\omega} > n_{\omega}$.

When both absorption and diffusion are absent, the intensity of the second harmonic obtained for sample depends on the phase mismatch $\Delta\Psi$:

$$\Delta\Psi = \Delta k\, L = \left(\frac{4\pi\,\Delta n}{\lambda_{\omega}}\right)L = \left(\frac{\pi}{L_c}\right)L \quad (5)$$

with

$$\Delta n = n_{2\omega} - n_{\omega} \text{ and } L_C = \frac{\lambda_{\omega}}{4(n_{2\omega} - n_{\omega})} \quad (6)$$

where λ_{ω} denotes the length of fundamental wave and L_c - the coherence length equal to the distance at which a phase mismatch equal to π is accumulated between the constraint and free waves of the second harmonic.

Jerphagnon and Kurtz are the first who published a theoretical description of the fringes [25] observed initially by Maker in 1962 [24]. They considered that the intensity of the second harmonic induced by propagation of the fundamental wave through a nonlinear material on the emerging phase is given by the relation:

$$I_{2\omega} = I_M(\theta)\sin^2\Psi \quad (7)$$

Where

$$\Psi = \frac{2\pi}{\lambda_{\omega}}(n_{\omega}\cos\theta_{\omega} - n_{2\omega}\cos\theta_{2\omega})L \approx \frac{\pi}{2}\frac{L}{L_c(\theta)} \quad (8)$$

Denotes the interference factor between the constraint and free waves, and $L_c(\theta)$ the coherence length depending on the angles θ_{ω} and $\theta_{2\omega}$.

The overlapping of Maker fringes, $I_M(\theta)$, is given by:

$$I_M(\theta) = \left(\frac{1}{n_{2\omega}^2 - n_{\omega}^2}\right)^2 \left(d_{eff}(\theta)\right)^2 I_{\omega}^2\left(t_{\omega}(\theta)\right)^4 T_{2\omega}(\theta) \quad (9)$$

Where $d_{eff}(\theta)$ is the projection of the effective nonlinear coefficient on the electric field of the fundamental wave $t_{\omega}(\theta)$ and $T_{2\omega}(\theta)$ are related to the transmission coefficients (Fresnel coefficients) at the frequencies ω and 2ω, respectively. If the component of the second harmonic wave (polarized horizontally – *p*, parallel to incidental plane) is observed and of the fundamental wave is polarized vertically (*s*) (perpendicular to incidental plane), the transmission coefficients are given by the following relations:

$$t_{\omega}(\theta) = \frac{2\cos\theta}{n_{\omega}\cos\theta_{\omega} + \cos\theta} \quad (10)$$

$$T_{2\omega}(\theta) = \frac{2\,n_{2\omega}\cos\theta_{2\omega}(\cos\theta + n_{\omega}\cos\theta_{\omega})(n_{\omega}\cos\theta_{\omega} + n_{2\omega}\cos\theta_{2\omega})}{(n_{2\omega}\cos\theta_{2\omega} + \cos\theta)^3} \quad (11)$$

In the case of polarization *p* of the fundamental wave, they are:

$$t_{\omega}(\theta) = \frac{2\cos\theta}{n_{\omega}\cos\theta + \cos\theta_{\omega}} \quad (12)$$

$$T_{2\omega}(\theta) = \frac{2\,n_{2\omega}\cos\theta_{2\omega}(\cos\theta_{\omega} + n_{\omega}\cos\theta)(n_{\omega}\cos\theta_{2\omega} + n_{2\omega}\cos\theta_{\omega})}{(n_{2\omega}\cos\theta + \cos\theta_{2\omega})^3} \quad (13)$$

By choosing the polarization states for input and output wave, it is possible, by using an appropriate theoretical model, to tune the value of effective nonlinear coefficient d_{eff} until the partitions of fringes experimentally obtained are well fitted.

In this way, we obtain some information on the interference order, and thus, on the coherence length. For calibration of the experimental setup 0.5 mm Y-cut quartz has been used as reference material (d_{11} = 0.5 pmV^{-1}, $L_c \approx$ 20.5 μm) [26].

In the case of a nonlinear material thin layer deposited on a centrosymmetric substrate with different refraction indices, we have to take into account the modification of the transmission coefficients through a layer/substrate interface which replaces the layer/air interface, while the substrate/air interface is added. The new transmission coefficient for a second harmonic wave is written as follows:

$$T'_{2\omega} = \left\{ \left[T_{2\omega}(\theta) \right]_{(n_{air} \to n_{substrat})} \right\} \times T_{2\omega}^{substrat/air}, \tag{14}$$

where:

$$T_{2\omega}^{substrat/air} = \frac{2n_{2\omega}^{substrat} \cos\theta_{2\omega}^{substrat}}{\cos\theta_{2\omega}^{substrat} + n_{2\omega}^{substrat} \cos\theta_{2\omega}^{exit}} \tag{15}$$

either by replacing in equation (14) for a polarization *s* of the fundamental wave:

$$T'_{2\omega}(\theta) = \frac{2n_{2\omega}\cos\theta_{2\omega}(\cos\theta + n_{\omega}\cos\theta_{\omega})(n_{\omega}\cos\theta_{\omega} + n_{2\omega}\cos\theta_{2\omega})}{(n_{2\omega}\cos\theta_{2\omega} + \cos\theta)(n_{2\omega}\cos\theta_{2\omega}^{substrat} + n_{2\omega}^{substrat}\cos\theta_{2\omega})^2} \tag{16}$$

or by replacing in equation (16) for a polarization *p* of the fundamental wave:

$$T'_{2\omega}(\theta) = \frac{2n_{2\omega}\cos\theta_{2\omega}(\cos\theta_{\omega} + n_{\omega}\cos\theta)(n_{\omega}\cos\theta_{2\omega} + n_{2\omega}\cos\theta_{\omega})}{(n_{2\omega}\cos\theta + \cos\theta_{2\omega})(n_{2\omega}\cos\theta_{2\omega}^{substrat} + n_{2\omega}^{substrat}\cos\theta_{2\omega})^2}. \tag{17}$$

3. 2.2. 1. Theoretical models

The main literature models exhibit their particular specificity depending on the type of sample to be characterized: powder, solution, thin layer, bulk material, etc.

3. 2.2. 2. Kurtz and Perry model

The simplified model of Kurtz and Perry [27], developed for microcrystalline powders, is based on the comparison of macroscopic NLO properties of the sample studied to those of a reference material (generally a brown powder called POM (3-methyl-4-nitropyridine-1-oxide)):

$$\frac{\chi^{<2>}}{\chi_{POM}^{<2>}} = \sqrt{\frac{I^{2\omega}}{I_{POM}^{2\omega}}}, \tag{18}$$

where $\chi^{<2>}$ and $\chi_{POM}^{<2>}$ denote the second order nonlinear susceptibilities of studied material and POM ($\chi_{POM}^{<2>}$ = 12.0 pmV^{-1} [28]), respectively, while $I^{2\omega}$ and $I_{POM}^{2\omega}$ are the maximal intensities of the second harmonic signal of the studied material and POM, respectively.

The major inconvenience of this model is the strong crystallinity influence during the measurements of second harmonic signal intensity. Actually, the size of the crystallites influences the phase accord and, consequently, the second harmonic signal intensity. In this case, it is indispensable to know exactly the crystallite size.

3. 2.2. 3. Lee model

The simplified model of Lee *et al*. [29] is used for thin layers and is based on comparison of macroscopic NLO properties of the sample under study to those of 0.5 mm thick Y-cut quartz, taking into account particularly of the film thickness, *d*, and its coherence length of quartz $l_{c,q}$:

$$\frac{\chi^{<2>}}{\chi_q^{<2>}} = \frac{2}{\pi}\frac{l_{c,q}}{d}\sqrt{\frac{I^{2\omega}}{I_q^{2\omega}}}, \tag{19}$$

with:

$$l_{c,q} = \frac{\lambda_{\omega}}{4\left(n_{q(2\omega)} - n_{q(\omega)}\right)}, \tag{20}$$

where $\chi^{<2>}$ and $\chi_q^{<2>}$ denote second order nonlinear susceptibilities of the studied material and quartz ($\chi_q^{<2>}$ = 1.0 pm V^{-1} [30]), respectively, $I^{2\omega}$ and $I_q^{2\omega}$ - the second harmonic intensities of studied material and quartz, respectively, λ_{ω} - the wavelength of fundamental beam ($\lambda_{\omega} = 1064$ nm), $n_{q(\omega)}$ and $n_{q(2\omega)}$ the refractive indices of quartz at the wavelength of the fundamental and the second harmonic beam, respectively ($n_{q(\omega)}$ = 1.534 at 1064nm and $n_{q(2\omega)}$ = 1.547 at 532 nm [26]).

3. 2.2. 4. Model of Herman and Hayden

The model used in this study for characterization of bulk materials and thin layers is the model developed by Herman and Hayden in 1995 [31]. This model has been chosen since, contrary to previous two models, has the advantage to explicit of the second harmonic intensity by taking into account the materials' absorption. The second

harmonic wave (polarized horizontally - *p*) from the fundamental wave polarized vertically – *s* for nonlinear isotropic material may be expressed as follows [31, 32]:

$$I_{2\omega}^{s\to p}(\theta)=\frac{128\pi^5}{c\lambda^2}\frac{\left[t_{af}^{1s}\right]^4\left[t_{fs}^{2p}\right]^2\left[t_{sa}^{2p}\right]^2}{n_{2\omega}^2\cos^2\theta_{2\omega}}I_{\omega}^2\left(L\chi_{eff}^{(2)}\right)^2\exp\left[-2(\delta_1+\delta_2)\right]\frac{\sin^2\Phi+\sinh^2\Psi}{\Phi^2+\Psi^2} \quad (21)$$

where the reflexions are neglected and I_ω and λ denote the light intensity and the wavelength of the fundamental wave, respectively, $\chi_{eff}^{<2>}$ - effective second order nonlinear susceptibility, L - the film thickness, t_{af}^{1s}, t_{fs}^{2p} and t_{sa}^{2p} - transmission coefficients (system air-film-substrate-air) for fundamental and second harmonic beams. The phase angles Φ and Ψ may be expressed in the form:

$$\Phi=\frac{2\pi L}{\lambda}\left(n_\omega\cos\theta_\omega-n_{2\omega}\cos\theta_{2\omega}\right), \quad (22)$$

$$\Psi=\delta_1-\delta_2=\frac{2\pi L}{\lambda}\left(\frac{n_\omega\kappa_\omega}{\cos\theta_\omega}-\frac{n_{2\omega}\kappa_{2\omega}}{\cos\theta_{2\omega}}\right), \quad (23)$$

where θ_ω and $\theta_{2\omega}$ denote the angles between fundamental and the second harmonic beams, respectively, n_ω and $n_{2\omega}$ - the refraction indices of the fundamental and of harmonic waves, respectively, κ_ω and $\kappa_{2\omega}$ - the extinction coefficients of the nonlinear material at the angular frequencies ω and 2ω, respectively.

Using the Lee model the second order nonlinear optical susceptibility of the CdSe-PMMA nanocomposite system was determined from the SHG signal intensity recorded versus the incident angle varying from -50° to 50° (Fig. 4). For a constant input intensity and no dispersion, the effective quadratic nonlinear susceptibility, $\chi_{eff}^{<2>}$ of the thin film sample is related with that of the reference plate by following equation (24) [29] ,[33, 36]:

$$\left|\chi_{eff(f)}^{<2>}\right|=\left(\frac{2}{\pi}\right)\left(\frac{I_{(2\omega)}^{M}(f)}{I_{(2\omega)}^{M}(q)}\right)^{\frac{1}{2}}\frac{l_{c(q)}}{d_f}\left|\chi_{eff(q)}^{<2>}\right| \quad (24)$$

In which we assume $d_f << l_c(f)$ and $d_q >> l_c(q)$.

d_f is the sample thickness assumed to be thinner than the coherence length $l_c(f)$ and d_q is the thickness assumed to be thicker than the quartz substrate coherence length ($l_c(q)$). $I_{(2\omega)}^{M}$ Represents the SH intensity at the maximum of the envelope function (locus of the Marker fringe peaks). $I_{(2\omega)}^{M}(f)$, $I_{(2\omega)}^{M}(q)$ are the SH intensity maxima for the NCs doped film and quartz plate respectively.

From the experimental results, we obtained $\chi_{eff}^{<2>}$ =2.27.10^{-10} (m/V). This value is two orders larger than the reference material (1 pm/V) [37] and 4 times larger than that for the CdSe bulk material (52 pm/V) [38]. Our results are in line with the work of Katarzyna et al [39]. This result suggests a large influence on the quantum confinement due to the low dimensionality of the crystallites.

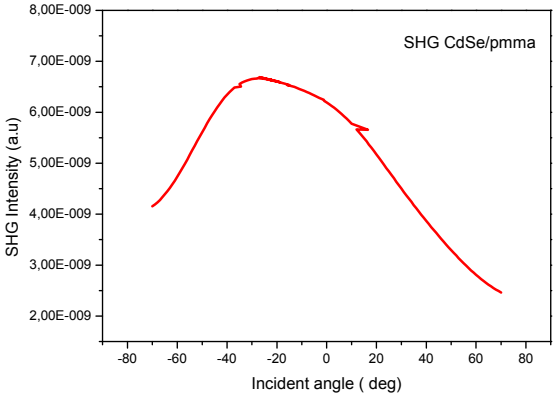

Fig. 6. SHG signal intensity dependence versus the incident angle of the fundamental beam for the CdSe-PMMA nanocomposite thin film (thickness=120 nm). The dotted curve represents the experimental data and the solid line the fitted curve

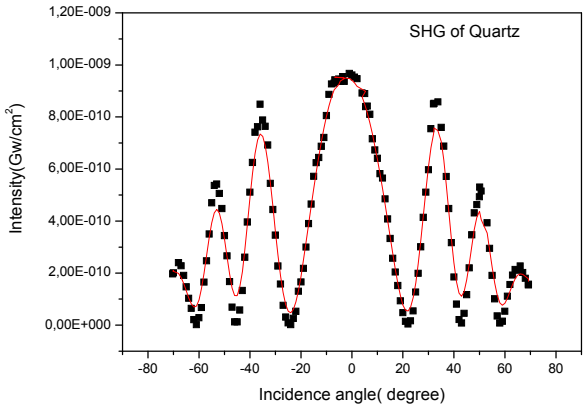

Fig. 7. SHG signal intensity of the signal versus incident angle of the fundamental beam of the reference (quartz).The dark points are the experimental values of the SH intensities, The solid line is the line obtained by fitting the experimental values.

3. 2.3. Principle of the third harmonic generation

Third Harmonic Generation (THG) technique consists in generating a wave of triple frequency 3ω starting from an incident beam of frequency ω. In fact, similarly to the SHG, generation of the third harmonic represents an optical interaction in which three photons of energy *hv* (in our case, λ_ω=1064 nm and *hv*=1.17eV) interact with nonlinear medium generated a new photon of energy 3*hv* (in our case, $\lambda_{3\omega}$ =355 nm and 3*hv*=3.51eV).We used for this investigation the Lee theoretical model

The effective nonlinear cubic susceptibility $\chi_{eff}^{<3>}$ of the NCs thin doped thin film is related with that of the reference sample through equation (25). [29]

$$\left|\chi^{<3>}{}_{eff}\right| = \left(\frac{2}{\pi}\right)\left(\frac{I_{(3\omega)}{}^{M}(f)}{I_{(3\omega)}{}^{M}(s)}\right)^{\frac{1}{2}} \frac{l_{c(s)}}{d_f}\left|\chi^{<3>}{}_{eff\,(s)}\right| \qquad (25)$$

Where $l_c(s)$ is the coherence length of the silica plate and $I_{(3\omega)}{}^{M}(f)$, $I_{(3\omega)}{}^{M}(s)$ are the TH intensity maxima for the thin film and the silica plate respectively. Using the equation (25) we calculated the values of $\chi_{eff}^{<3>} = 2.28\times10^{-20}$ (m^2/V^2) (see figure 8). This value is two orders higher than the reference (see figure 9) material (2×10^{-22} m^2/V^2) [40] and is also attributed to the quantum confinement effect.

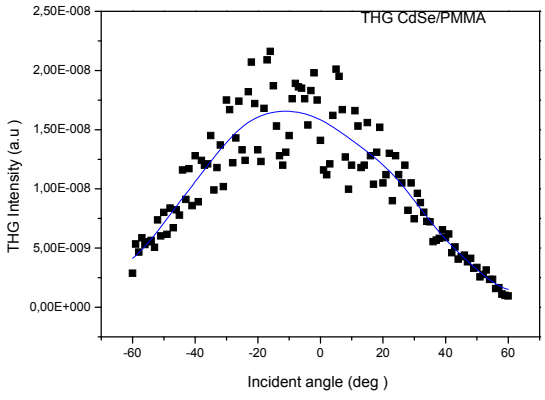

Fig. 8. THG signal intensity dependence versus incident angle of the fundamental beam for the CdSe-PMMA nanocomposite thin film (thickness=120 nm). The full squares curve represents the experimental data and the solid line the fitted curve.

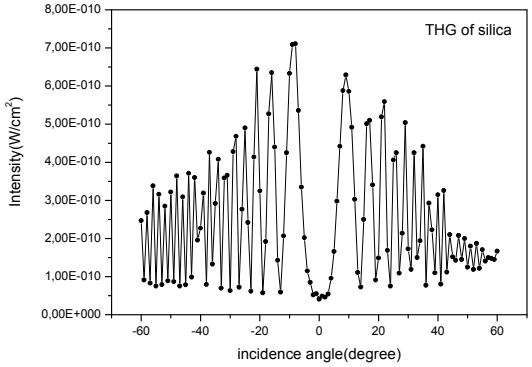

Fig. 9. Intensity of the signal THG versus incident angle of the reference silica.

3. 3. Atomic force microscopy images

The surface morphology was examined by AFM and showed that the matrix PMMA exhibits some homogeneous porosity and is able to accept the incorporation of the crystallites of CdSe (see figure 10). The roughness of the CdSe-PMMA film surface was quantified by the parameter RMS defined as the root means square average between the height deviations and the mean line/surface [41], taken over the evaluation length/area (i.e. over the scanned surface). A value of RMS = 6 nm was found. The AFM images (see figure 11), clearly show that the crystallites of CdSe are incorporated in the matrix and the film presents some homogeneous distribution over a wide range of the surface (see figure 11). The thickness of the film was estimated with AFM to be around 80-120nm (see figure 12) and confirmed the results obtained from the Dektak 6M stylus profiler (Veeco).

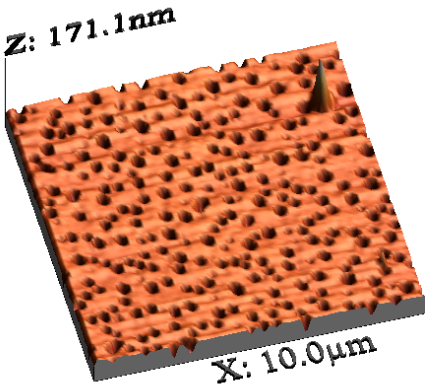

Fig. 10. AFM images of PMMA surface NCs incorporated in PMMA

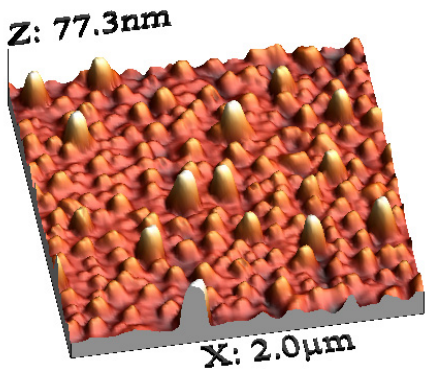

Fig. 11. AFM images of CdSe NCs incorporated in PMMA.

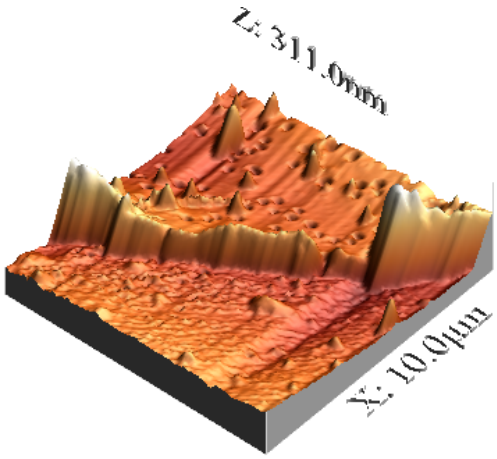

Fig. 12. AFM image use for estimation of the thickness (80-120 nm) CdSe-PMMA film.

4. Conclusions

The preparation of CdSe NCs using colloidal solution and their well incorporation in a PMMA matrix is reported and supported by complementary investigations. These CdSe NCs exhibit both a blue shift and discrete energy states at low crystallites size. A strong quantum confinement was established. Additionally, second and third order NLO investigations were performed using SHG and THG experiments and the corresponding NL susceptibilities $\chi_{eff}^{<2>}$ and $\chi_{eff}^{<3>}$ compared to those of the reference materials. In both cases, large values were obtained $\chi_{eff}^{<2>}$ = $2.27.10^{-10}$ m/V and $\chi_{eff}^{<3>}$ = 2.28 10^{-20} m^2/V^2. It has been shown that the reduction in size of the materials from bulk scale to the nanoscale semiconductor would lead to a large enhancement on the second and third optical nonlinearity. This enhancement of NL susceptibilities is potentially attributed to the quantum confinement effect of nanosized CdSe. We performed additional studies on other NCs semiconductors belonging to the same family II-VI (ZnSe, ZnO, and ZnS). The results regarding the second and third order susceptibility show the same behaviour. The increase is more pronounced for materials with larger energy gap. These features make the CdSe-PMMA thin films a very promising nonlinear optical material for devices and applications in optoelectronic and nanophotonic fields.

Acknowledgements

The authors acknowledge the Service Commun d'Imageries et Analyses Microscopiques of the University of Angers for performing AFM measurements.

References

[1] S. Nakamura, in: G.B. Stringfellow, M.G. Craford (Eds.), High Brightness Light Emitting Diodes, Academic Press, New York, **48,** 391 (1997).
[2] M. Yano, M. Okamoto, Y. K. Yap, M. Yoshimura, Y. Mori, T. Sasaki. Diamond and Related Materials, **9**, 512 (2000).
[3] L. Brus, Appl. Phys. A: Mater. Sci. Process. **53**, 465 (1991).
[4] C. Nadrian. Seeman and Angela, M Belcher. PNAS, **99**, 6451 (2002).
[5] H. Mattoussi, J. Mauro, E. Goldman, G. Anderson, V. Sundar, F. Mikulec, M. Bawendi, J. Am. Chem. Soc. **122**, 12142 (2000),
[6] C. Murray, C. Kagan, M. Bawendi, Annu. Rev. Mater. Sci. **30**, 546 (2000),
[7] A. Efros, Rosen, M. Annu. Rev. Mater. Sci. **30**, 475 (2000).
[8] U. Woggon, Optical Properties of Semiconductor Quantum Dots; Springer: New York, (1997).
[9] C. B. Murray, D. J. Norris,and M. G. Bawendi. J. Am. Chem. Soc. **115**, 8706 (1993),
[10] D. J. Norris A.L. Efros, M. Rosen G. Bawendi Phys. Rew. B. **53**, 16347 (1996).
[11] L. E. Brus, J.Chem.Phys. **79**, 5566 (1983).
[12] P. D. Maker, R.W. Terhune, M.F. Niseno, C. M. Savage, Phys. Rev. Lett. **8**, 2112 (1962).
[13] F. Kajzar, J. Messier, C. Rosilio, J. App. Phys. **60**, 3040 (1986).
[14] M. Alaoui Lamrani, M. Addou, Z. Sofiani, B. Sahraoui, J. Ebothé, A. El Hichou, N. Fellahi, J. C. Bernèche, R. Dounia Optics Communications **277,** 196 (2007).
[15] Z. Sofiani, B. Sahraoui M. Addou, R. Adhiri, M. Alaoui Lamrani, L. Dghoughi., N. Fellahi. J. Appl. Phys. **101**, 063104 (2007).
[16] T. Arai, K. Matsuishi, J. Lumin. **70,** 281 (1996).
[17] P. Nemec, D. Mikes, J. Rohovec, E. Uhlifova, F. Trojanek, P .Maly , Mater. Sci. Eng. **B69-70**, 500 (2000) .

[18] J. Joseph-Charles, M. Bertucat, P. Levillain, Bull. Soc. Pharm. Bordeaux, **136**, 56 (1997).
[19] Landolt-Börnstein, Handbook of Physics, vol. 17b, Springer, Berlin, (1982)
[20] Kayanuma.Y, Phys .Rev B **38**, 9797 (1988).
[21] L.E. Brus, J. Chem. Phys. **80**, 4403 (1984).
[22] Handbook, Physico-Chemical Properties of Semiconductor Compounds, Nauka, Moscow, 1979.
[23] M. Simurda, P. Nemec, P. Formanek, I. Nemec, Y. Nemcova, P. Maly, Thin Solid Films **503**, 64 (2006).
[24] P. Maker, R. Terhune, M. Nisenoff, C. Savage, Phys. Rev. Lett. **8**, 21 (1962).
[25] J. Jerphagnon, S. Kurtz, J. Appl. Phys. **40,** 1667 (1970).
[26] R. A. Myers, N. Mukherjee, S. R. J. Brueck, Opt. Lett. **16** 1732 (1991).
[27] S. K. Kurtz, T. T. Perry, J. Appl. Phys. **39,** 3798 (1968).
[28] M. Guillaume, E. Botek, B. Champagne, F. Castet, L. Ducasse, J. Chem. Phys. **121,** 7390 (2004).
[29] G. J. Lee, S. W. Cha, S. J. Jeon, S. I. Jin, J. Kor. Phys. Soc. **39,** 912 (2001).
[30] F. Kajzar, Y. Okada-Shudo, C. Meritt, Z. Kafafi, Synth. Met. **117,** 189 (2001).
[31] W. Herman, L. Hayden, J. Opt. Soc. Am. B **12,** 416 (1995).
[32] B. Kulyk, Z. Essaidi, J. Luc, Z. Sofiani, G. Boudebs, G. Sahraoui, V. Kapustianyk, B. Turko J. Appl. Phys. **102,** 113113 (2007).
[33] S. K. Kurtz, Quantum Electronics: a Treatise, edited by Rabin, H. and Tang, C. L. (Academic Press, New York, 1975), p. 263.
[34] J. Jerphagnon, S. K. Kurtz, J. Appl. Phys. **41**, 1667 (1970).
[35] B. Kulyk, Z. Essaidi, J. Luc, Z. Sofiani, G. Boudebs, B. Sahraoui, V. Kapustianyk and B. Turko J. Appl. Phys. **102**, 113113, (2007).
[36] G. J. Lee, S. K. Yu and D. Kim, J .Opt. Soc. Korea **5**, 18 (1994).
[37] J. Geoffrey. Ashwell and Mukhtar A. Amiri, J. Mater.Chem **12**, 2181 (2002).
[38] Hand book of optic materials. 2003 by CRC Press LLC (2003).
[39] O. Katarzyna et al Journal of Nano Research **2,** 31 (2008).
[40] U. Gubler and C.Bosshard . Phys. Rev. **B 61**, 10702 (2000).
[41] V. Kapustianyk, B. Turko, A. Korstruka, Z. Sofiani, B. Derkowska, S. Dabos-Seignon, B. Barwinski, Yu. Eliyashevskyi, B. Sahraoui. Optics Communications **269**, 346 (2007).

*Corresponding author: bouchta.sahraoui@univ-augers.fr